Deep Learning Method for Fault Diagnosis in High Voltage Transmission Lines: A Case of the Vietnam 220kV Transmission Line

Le Van Dai[1]*, Nguyen Nhan Bon[2], and Le Cao Quyen[3]

[1]Electric Power System Research Group,
Industrial University of Ho Chi Minh City, Ho Chi Minh City, Vietnam
[2]Faculty of Electrical and Electronics Engineering,
Ho Chi Minh University of Technology and Education, Ho Chi Minh City, Vietnam
[3]Power Engineering Consulting Joint Stock Company 4,
Nha Trang City, Khanh Hoa province, Viet Nam
levandai@iuh.edu.vn, bonnn@hcmute.edu.vn, rdc@pecc4.vn
*Corresponding author: levandai@iuh.edu.vn

Abstract: One of the significant obstacles in electrical power transmission is the incident of failures, most notably the fault in transmission lines. It can influence the quality of the supplied electrical power, and actually, the country's security and economy are threatened. Researching an intelligent solution to diagnose the fault is the done thing. This paper integrates deep learning methods, namely the discrete wavelet transform (DWT), GoogleNet, and probabilistic neural network (PNN) approaches, to detect, classify, and locate the fault. The DWT-based multi-resolution analysis (MRA) is used for fault identification to process energy distribution during the transient states. After feature extraction, the obtained energy of the subband signal is used as the feature vector. It is employed as an input of GoogleNet for the fault type classification. The effectiveness of the proposed method has been demonstrated on the 220kV transmission line between the Hoa Khanh and Hue substations of Vietnam via time-domain simulation using EMTP-RV and MATLAB softwares. The simulated results are compared to the accuracy of the line distance protection REL521 for considering even cases, including the normal case and ten different fault causes, and the conditions of the pre-fault load changes. As a result, it concludes that the proposed method is a favourable method applied to the problem of analyzing the power system stability in the field of power transmission.

Keywords: Deep learning; discrete wavelet transform (DWT); GoogleNet, and probabilistic neural network (PNN); fault diagnosis; Vietnam 220-500 kV Transmission line.

1. Introduction

The electric power transmission network is a connection between multi-source and -load. It is the most important link in the country's energy system. As the country develops, demand for electricity increases, leading to more distributed distribution sources, and electrical loads are connected to the existing power network. Therefore, complexity is increasing in all areas of the electrical system, resulting from the disturbance or fault, especially electrical faults. The causes of faults are weather conditions, missed operation, overload, equipment failures, human errors, and smoke of fires. The power systems have faced severe blackouts due to technical, human, and electrical faults in the past decades. The effects caused by them are the overcurrent flow, danger to person, equipment loss, economic loss, and national security. The faults are Single line to ground (SLG), line to line (LL), double line to ground (LLG), three-line (LLL), and three-line to ground (LLLG) faults. For a three-phase electrical power system, all of the fault categories were expanded to ten different fault forms on transmission lines. The conjecture of faults is shown in Figure 1 [1], in which 50% of faults can occur in the transmission lines as shown in Figure 1 (a), and 85% of SLG faults can occur as shown in Figure 1 (b). Therefore, it is important to accurately identify, classify, and locate faults on high voltage transmission lines for the reliable operation of power system networks.

Received: March 26th, 2022. Accepted: June 25th, 2022
DOI: 10.15676/ijeei.2022.14.2.1

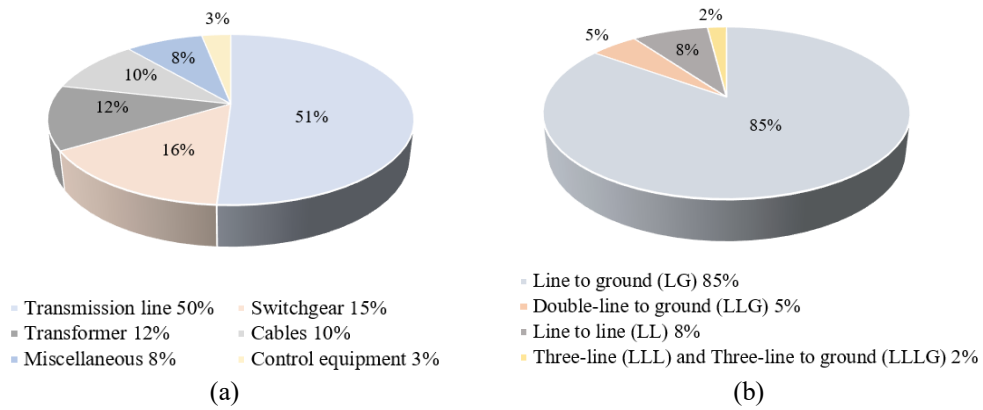

Figure 1. The conjecture of faults: (a) The possibility of fault on the various parts of the electric system, (b) The occurred probability of different types of fault

The methods related to fault detection, location, and classification on the transmission line have been introduced and applied over the past couple of decades. These methods are based on the current and voltage signals measured at the transmission line terminal. In turn, the one-end algorithm has been introduced in [2,3] and applied by Toshiba, Siemens, and ABB. This technique uses the multifunction digital relay based on the measured fundamental frequency voltages and currents at one end of the lines is the most popular. In particular, the accurate fault location of Toshiba, Siemens, and ABB is ± 2.5 %, ≤ 2.5%, and 2.5 of the line length, respectively [4]. It does not have sufficient accuracy because it does not consider fault resistance and inception angle. Furthermore, this method's accuracy is reduced when the line is connected to another terminal [5]. Authors in [6] presented the algorithm that two-end currents and voltages are measured synchronously by applying phasor measurement units (PMUs). Due to the measurement of current and voltage signals at both ends of the transmission line. Accordingly, this method has a high computational time. However, it can improve the accuracy of locating the fault. The method based on the travelling wave has been developed in [7]. Authors have used the interdependence of for- and back-ward waves travelling in the transmission line. The optimization of this method is less error when locating the fault in case of high fault resistance. However, the main disadvantage is a high computational time.

Currently, the methods mentioned earlier face significant errors and high computational time due to the complexity of the fault modelling on different fault types. Several published studies are related to fault detection, location, and classification on the transmission line to overcome these problems. Saravanababu et al. [8] proposed the discrete wavelet transform (DWT) method to extract the hidden factors from ten different faults by applying decomposition at different levels. This method is also used as an online relay protection tool [9]. The artificial neural network (ANN) method is a type of learning algorithm and the nonlinear statistical model used to simulate the behaviour of connected neurons in biological neural systems. Authors in [10] used this method to diagnose the actual transmission line fault. In this method, the authors proposed the discrete Fourier transform to decompose the measured fault voltages and currents signals that are fed as inputs to the neural network. As a result, the ability to learn through training is the ANN's strength. However, this ability's efficacy depends on the level of training. The fuzzy logic (FL) method [11] used language variables rather than numerical ones, making the process easier. However, accuracy in fuzzy logic-based systems is not guaranteed for wide variations in system conditions.

In recent years, using the wavelet transform (WT) was combined with other methods extensively to study the fault diagnosis in high voltage transmission lines. For example, a combination of the WT and FL was proposed by Jamil et al. [11]. In this work, the fuzzy method based on the DWT was used to identify the ten different types, considering the effect of variation in fault inception angle, loading, and other parameters. This method, using the WT to decompose

the signals and applying the FL based on the rules to give fault types, was developed by Ray et al. [12]. Authors in [13,14] have presented a fault classification and location method on power transmission lines based on a combination of the WT and support vector machines (SVM). Another combination of the WT is with ANN developed by Baqui et al. [15]. The authors used the WT to extract relevant information from the current signals and then used ANN to train. The authors also use this method in [16] to identify and classify faults. However, these combined methods need a large number of samples and training, which can increase the complexity. Several other methods that are also quite successful in protecting transmission lines are synthesized and compared by authors in [17,18].

The WT method was developed in the 1980s and applied in many different fields, including signal processing of accelerations to analyze the gait, detect the fault, design the low power pacemakers, etc. For each other suitable applications, there are a large number of wavelet transforms such as the continuous WT (CWT), DWT, multiresolution-based WT, Fast WT, stationary WT, fractional WT, etc. Among them, the DWT is chosen as an optimal solution for the case of transient analysis in the power system [19,20]. The GoogleNet was developed by Szegedy et al. 2014 for the ImageNet Large-Scale Visual Recognition Challenge 2014 (ILSVRC 2014). GoolgeNet model is a type of convolutional neural network (CNN) built based on three parts. The first one uses layers the same as the architecture of AlexNet and LeNet, containing a series of one 7×7 convolutional, two 3×3 Maxpool, one 1×1convolutional, and one 3×3 convolutional layers; the second one uses nine inception layers broken into three blocks (2×, 5× and 2×) by two Maxpool layers to reduce the dimension; and the third one is the classification part of the network consisting of the linear, softmax, and global AvgPool [21,22]. The GoogleNet has been widely used in image classification, pattern recognition, and other fields [23–25]. From a technical point of view, GoogleNet can extract more features under the same computing. It is more efficient in computation time and improves the training results than the AlexNet, AGGNets, ResNet, and other Net. The probabilistic neural network (PNN) is first introduced by Specht [26]. This network has a simple structure built based on Bayes classification rules and the Parzen window probability density function estimation method. In practical application, it has advantages, particularly to be classification issues; the linear learning algorithm in PNN is capable of reaching the results of nonlinear learning algorithms while keeping the nonlinear algorithm's high accuracy. In recent years, the PNN has also been researched for fault diagnosis. Akram et al. [27] have applied the PNN to detect and classify the real-time open- and short-circuit faults. Some other applications as the classification of power quality, voltage sag, etc., were studied in [28–31].

Although the DWT, GoogleNet, and PNN methods have various advantages mentioned above. This study proposes an integration of the three these deep learning methods to identify, classify, and locate other fault types on high voltage transmission lines. The DWT-based multi-resolution analysis (MRA) is used for fault identification to process energy distribution during the transient states. After feature extraction, the obtained energy of the subband signal (decomposed by DWT) is transferred under the feature vector form. It is employed as an input of GoogleNet for the fault type classification. The PNN is used to locate the fault after successfully classifying. However, the PNN proposes to locate the fault having some disadvantages. For example, the memory requirement is large, and the recording time is proportional to the size of the sample. This paper applied Parseval's theorem to overcome these disadvantages.

The original contribution of this research is the development of a hybrid method combining the DWT, GoogleNet, and PNN methods applied to diagnose the faults on transmission lines. This proposed method can identify, classify, and locate the unsymmetrical and symmetrical faults under the conditions of the pre-fault load changes and the fault resistance random values. In addition, the RGB color image is used to diagnose the faults.

The paper consists of five Sections. The study motivation, background and related work, primary contributions, and organization are analyzed and presented in this Section 1. Section 2 demonstrates the DWT, GoogleNet, and PNN methods that advantage an algorithm to identify,

classify and locate the faults on the transmission line. The proposed combination algorithm of these methods is detailed in Section 3. Section 4 carries out the experiments and comparisons based on the Viet Nam 220 kV transmission line. Section 5 concludes the research work.

2. Methodological

A. The Wavelet Transform

1) The Discrete Wavelet Transform: The WT technique was extensively developed in the 1980s and used in the applied mathematics field for image and signal processing. The WT is divided into the DWT and CWT. The use of the DWT is more straightforward and requires less calculated weight over the CWT for analyzing the transient signals in the power system. For this study, the DWT is chosen as an optimal solution. Figure 2 illustrates the multi-resolution of DWT for the input signal $x[t]$ (current or voltage) to the continuous-time in terms of detailed and approximated versions under different frequency resolution levels

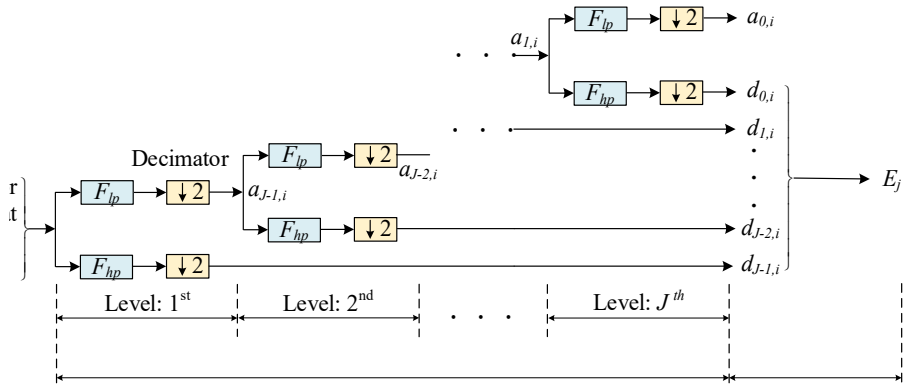

Figure 2. The processing solution of distribution energy

The approximated and detailed versions at the analytic hierarchy j can be calculated, respectively, as follows:

$$a_{j,i} = \int_{-\infty}^{\infty} x[t] s_{j,i}[t] dt \tag{1}$$

$$d_{j,i} = \int_{-\infty}^{\infty} x[t] w_{j,i}[t] dt \tag{2}$$

where $s_{j,i}[t]$ and $w_{j,i}[t]$ are the coefficients of scale and wavelet, respectively. Assuming that the mother wavelet function is expressed by Eq. (3), $s_{j,i}[t]$ *and* $w_{j,i}[t]$ can be defined by Eqs. (4) and (5), respectively.

$$w_{\tau,s}[t] = \frac{1}{\sqrt{|s|}} w[\frac{t-\tau}{s}] \tag{3}$$

$$s_{j,i}[t] = 2^{j/2} s[2^j t - i] \tag{4}$$

$$w_{j,i}[t] = 2^{j/2} w[2^j t - i] \tag{5}$$

where $j \in Z$ and $i \in Z$ are the analytic hierarchy and the operational index, respectively. With a set of obtained functions $s_{j,i}[t]$ *and* $w_{j,i}[t]$ in Eqs. (4) and (5), a function $x[t]$ can be expressed by Eq. (6). Observing this equation that the first part has $a_{j,i}$ presented the approximation with the resolution of one point for every $N=2^J$ points of the input signal $x[t]$ to the continuous-time.

Meanwhile, the second part has $d_{j,i}$ presented the detail of the input signal $x[t]$ to the continuous-time with different levels of resolution. Note that $d_{j,i}$ increases with j.

$$x[t] = \sum_j a_{j,i} s_{j,i}[t] + \sum_i \sum_{j=0}^{J-1} d_{j,i} w_{j,i}[t] \tag{6}$$

The corresponding relationship of approximation functions and detail between two adjacent analytic hierarchies j and (j+1) are respectively calculated in Eqs. (7) and (8) by using the Mallet method, where F_{lp} and F_{hp} are the low-pass and high-pass filters, and can be calculated by using MATLAB software. The limitation of F_{lp} is chosen in a range from zero to the frequency of $x[t]$ divided by 2^{J-j+1}, and the limitation of F_{hp} is chosen in a range from the frequency of $x[t]$ divided by 2^{J-j+1} to the frequency of $x[t]$ divided by 2^{J-j}. The relationship between J and j is shown in Figure 2.

$$a_{j,i} = \sum_k F_{lp}[k-2i] a_{j+1}[t], \quad 0 \le k \le \frac{N}{2^j} - 1 \tag{7}$$

$$d_{j,i} = \sum_k F_{hp}[k-2i] a_{j+1}[k], \quad 0 \le k \le \frac{N}{2^j} - 1 \tag{8}$$

This study assumes that the measured voltage or current signal after sampling with the number of sampling points of $N = 2^J$ is $x[t] = (x_0, x_1, x_2, \ldots, x_{n-1})$. The DWT of the measured signal at j^{th} analytic hierarchy decomposed between two adjacent analytic hierarchies j and (j + 1) as follows:

$$\mathrm{DWT}\left(x_j[t]\right) = 2^{\left(\frac{j+1}{2}\right)} \left(\sum_i a_{j,i} s[2^{(j+1)} t - i] + \sum_i d_{j,i} w[2^{(j+1)} t - i] \right), 0 \le i \le \frac{N}{2^j} - 1 \tag{9}$$

2) Parseval' Theorem for DWT: Assuming that the discrete current or voltage signal $x[t]$ flows through the resistance with a value of 1 Ohm, total consumptive energy on the resistance can be calculated by summing the Fourier spectrum coefficients and can be obtained in Eq. (10), where N is the number of sampling points and a_i is the spectrum coefficients. The contained energy in Parseval's theorem can be divided with the operational index i and the analytic hierarchy j as calculated in Eq. (11), that derived from Eqs. (9) and (10).

$$\frac{1}{N} \sum_{t=N} |x[t]|^2 = \sum_{i=N} |a_i|^2 \tag{10}$$

$$\frac{1}{N} \sum_t |x[t]|^2 = \frac{1}{N_j} \sum_i \left| s_{j,i} \right|^2 + \sum_{j=1}^{J} \left(\frac{1}{N_j} \sum_i \left| w_{j,i} \right|^2 \right) \tag{11}$$

3) Feature Extraction: In general, the transient duration and distribution energy are two factors that need to be used to detect and classify faults.

For the transient period: when a fault occurs, a discontinuity signal of the disturbance period is generated due to the stable power signal. When applying the DWT-MRA at one-level decomposition to analyze the distortional signal, it engenders the detail coefficients at the start and end time of the disturbance to create severe variation. It can easily detect the disturbance even. The transient period of the disturbance can be easily calculated using Eq. (12) by observing the variations in absolute detail coefficients, where t_s and t_e are the start and end times of the disturbance, respectively.

$$\tau = \left| t_e - t_s \right| \tag{12}$$

For distribution energy: after detection of the disturbance duration, the next important task is to determine the energy of the subband signal. The equation (11) shows that the energy of the distorted signal can be separated at various resolution levels in other ways that depend on different faults. Thus, this study will investigate the detailed coefficients at each resolution level to extract the features of the distorted signal for the classification of different fault types. The energy of the detail of the subband signal at the analytic hierarchy j and the energy of the approximation of the subband signal at the analytic hierarchy "0" can be obtained using Eqs. (13) and (14), respectively [32].

$$E_{d_j} = \left\| d_j \right\|_2 = \sqrt{\sum\nolimits_i \left| d_{j,i} \right|^2} \tag{13}$$

$$E_{a_0} = \left\| a_0 \right\|_2 = \sqrt{\sum\nolimits_i \left| a_{0,i} \right|^2} \tag{14}$$

The energy of the approximation of the subband signal, including the coefficients of scale and wavelet, can be obtained as follows

$$E = \left[\left\| a_0 \right\|_2 \ \left\| d_0 \right\|_2 \ \left\| d_1 \right\|_2 | \ldots | \left\| d_{J-2} \right\|_2 \ \left\| d_{J-1} \right\|_2 \right] \tag{15}$$

Therefore, after feature extraction, the obtained energy of the subband signal in Eq. (15) is used as the feature vector and is employed as an input of GoogleNet to classify the fault type.

B. *The GoogleNet*

The GoogLeNet model is chosen for this study with architecture, as shown in Figure 3. This architecture was proposed in the ILSVRC14 and was developed by a group of researchers at Google [33]. In general, this architecture is another form of conventional CNN. It is a pre-trained model having 22 layers. In order to simplify the work, this study is going to separate the GoogLeNet model into three parts. The first part (Part I), using layers the same as the architecture of the AlexNet and LeNet, contained a series of one 7×7 convolutional, two 3×3 Maxpool, one 1×1convolutional, and one 3×3 convolutional layers; the second part (Part II), using nine inception layers, broken into three blocks (2×, 5× and 2×) by two Maxpool layers to reduce the dimension; and the third part (Part III) is the classification part of the network consisting of the linear, softmax, and global AvgPool.

All the convolution, reduction, and projection layers apply the rectified linear unit (ReLU) non-linearity. The reduction and projection layers have used the average pooling layer to replace the fully connected layers, whereas the first few inception modules have used auxiliary classifiers. For this purpose, it can combat the vanishing gradient and overfitting problems. The input of GoogleNet is the RGB color image having the size of 224×224×3. The GoogleNet architecture in Figure 3 (a) is used in this study, and the detailed inception module is shown in Figure 3 (b). Its hyperparameters are set up as listed in Table 1.

C. *The Probabilistic Neural Network*

The PNN was developed by Specht [26] to be a type of monitor learning network and multilayer neural network. The basic topology of PNN is depicted in Figure 4. The PNN model includes the radial basis and the competitive layers applied in this paper. The radial basis layer evaluates the vector distance between the input and row weight vectors in the weight matrix. The obtained vector distances are scaled. The competitive layer is used to find the shortest distance from obtained distances. Finally, the training pattern closest to the input pattern is found based on these distances.

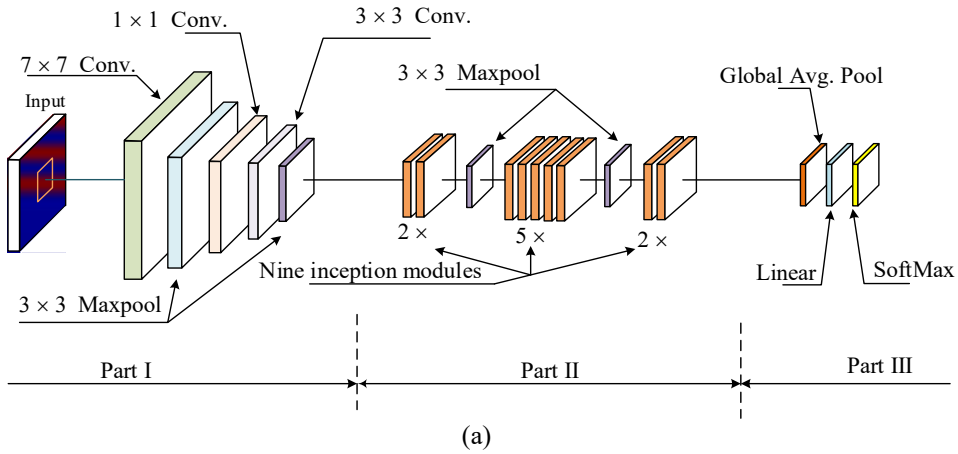

Figure 3. The GoogLeNet architecture: (a) The full GoogleNet model, (b) The detailed inception module of GoogLeNet

Table 1. The implemented hyperparameters of GoogLeNet

Type		Patch size	Output size	Depth	#1×1	#3×3 reduce	#3×3	#5×5 reduce	#5×5	Pool proj	Params	Ops
Part I	Convolution	7×7/2	112×112× 64	1							2.7K	34M
	Max pool	3×3/2	56×56× 64	0								
	Convolution	3×3/1	56×56× 192	2		2	2	2	2	2	124K	360M
	Max pool	3×3/2	28×28× 192	0								
Part II	Inception#1		28×28× 256	2	64	96	128	16	32	32	159K	128M
	Inception#2		28×28× 480	2	128	128	192	32	96	64	380K	304M
	Max pool	3×3/2	14×14× 480	0								
	Inception#3		14×14× 512	2	192	96	208	16	48	64	364K	73M
	Inception#4		14×14× 512	2	160	112	224	24	64	64	437K	88M
	Inception#5		14×14× 512	2	128	128	256	24	64	64	463K	100M
	Inception#6		14×14× 528	2	112	144	288	32	64	64	580K	119M
	Inception#7		14×14× 832	2	256	160	320	32	128	128	840K	170M
	Max pool	3×3/2	7×7× 832	0								
	Inception#8		7×7× 832	2	256	160	320	32	128	128	1072K	54M
	Inception#9		7×7× 1024	2	384	192	384	48	128	128	1388K	71M
Part II	Global Avg. Pool	7×7/2	1×1× 1024	0								
	Linear		1×1× 1000	1							1000K	1M
	Soft Max		1×1× 1000	0								

The training data set has n_k observations. The input layer contains three neurons for three dimensions of observation X, which can be calculated by using Eq. (16). The input layer is directly connected to the pattern layer via the centers C_{ih}, which can be calculated by using Eq. (17). The smoothing parameter σ, which should be adjusted experimentally and can set to be 0.5 for this study. The first and third centers have the label of "1" and the rest centers have the label "0", wherefore, the pattern layer divides two groups enclosing one group "H_1 and H_3" and

another group " H_2 and H_4 ". The distance between k^{th} observation $X^k = [x_1^k, x_2^k, x_3^k]$ and m^{th} center $C^m = [c_1^m, c_2^m, c_3^m]$ can be calculated in Eq. (18). The results of m^{th} pattern neuron for k^{th} observation can be obtained in Eq. (19). The first summation neuron can be obtained as $O_{k1} = \frac{1}{2} H_{k1} + \frac{1}{2} H_{k3}$ to correspond with label "1" and if O_{k2} is smaller O_{k1}, the prediction of kth observation is equal to "1" and otherwise, it is equal to "0".

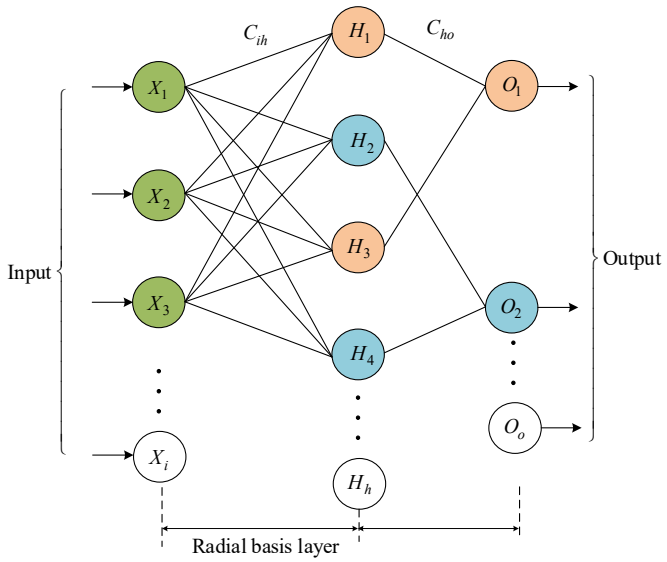

Figure 4. The topology of the probabilistic neural network (PNN)

$$X = \begin{bmatrix} x_1^1 & x_2^1 & x_3^1 \\ \vdots & \vdots & \vdots \\ x_1^{n_k} & x_2^{n_k} & x_3^{n_k} \end{bmatrix} \tag{16}$$

$$C_{ih} = \begin{bmatrix} c_1^1 & c_2^1 & c_3^1 \\ c_1^2 & c_2^2 & x_3^2 \\ c_1^3 & c_2^3 & x_3^3 \\ c_1^4 & c_2^4 & x_3^4 \end{bmatrix} \tag{17}$$

$$\left\| X^k - C^m \right\| = \sqrt{\left(x_1^k - c_1^m\right)^2 + \left(x_2^k - c_2^m\right)^2 + \left(x_3^k - c_3^m\right)^2} \tag{18}$$

$$H_{km} = e^{-\left(\frac{\|X_k - C_m\|^2}{\sigma^2}\right)} \tag{19}$$

The PNN model learns to approximate the probability density function of the training samples. More precisely, it can say that the PNN model is a function that approximates the probability distribution density of the fundamental samples. The PNN assumes all dimensions of observations are individual, and each default and non-default probability follow a mean of

multiple Gaussian distributions. The probability density function (*PDF*) of Gaussian distribution is calculated using Eq. (20) with considering a given mean μ, and smoothing parameter σ.

$$PDF[X] = \frac{1}{\sqrt{2\pi \square \sigma \square^2}} e^{-\left(\frac{\|X-\mu\|^2}{2\sigma^2}\right)} = \alpha X_{km} \tag{20}$$

For the application of the signal classification, the distribution values of training examples (k) are classified based on *PDF*. The equation (20) can be rewritten under the full form as follows [34]:

$$PDF[X] = \frac{1}{n_k} \sum_{o=1}^{n_k} e^{-\left(\frac{X-X_{ko}}{2\sigma^2}\right)} \tag{21}$$

The equation (19) can be rewritten under the full form as follows

$$H_h = e^{-\left(\frac{\sum_i \left(X_i - C_{ih}\right)^2}{2\sigma^2}\right)} \tag{22}$$

where i, h, and o are the number of inputs, hidden, and output layers, respectively. C_{ho} is the connection between the input and hidden layers. C_{ih} is the connection between the hidden and output layers.

The inference of the output layer can propose the following algorithm

Algorithm

$$\textit{Calculate: } \text{net}_o = \frac{1}{N_o} \sum_h C_{ho}.H_h$$

$$\text{and } N_o = \sum_h C_{ho},$$

$$\textit{if } \text{net}_o = \max_k (\text{net}_k)$$

$$\textit{then } O_o = 1$$

$$\textit{else } O_o = 0$$

In addition, using the PNN for locating the fault has some disadvantages, such as the memory requirement being large and the recording time being proportional to the size of the sample. In order to overcome disadvantages, Parseval's theorem is proposed to reduce the training input signals.

This study uses the energy level decomposition of each discrete distorted signal (current or voltage), which is obtained by applying DWT to determine the detailed coefficients ($d_{1,i}, d_{2,i}, \ldots, d_{13,i}$). The equatons (13) and (14) are used to calculate the energy of the detail of the subband signal at the analytic hierarchy ($j = 0, \ldots, 13$) and the energy of the approximation of the subband signal at the analytic hierarchy "0". The transient period of the disturbance can be calculated by using Eq. (12).

3. Proposed Algorithm

The proposed method for detecting, classifying, and locating the faults in the transmission line is developed from three deep learning methods of the DWT, GoogleNet, and PNN were analyzed in Section 2. The flowchart of the proposed method is described in Figure 5, and the procedure can be performed in the following steps:

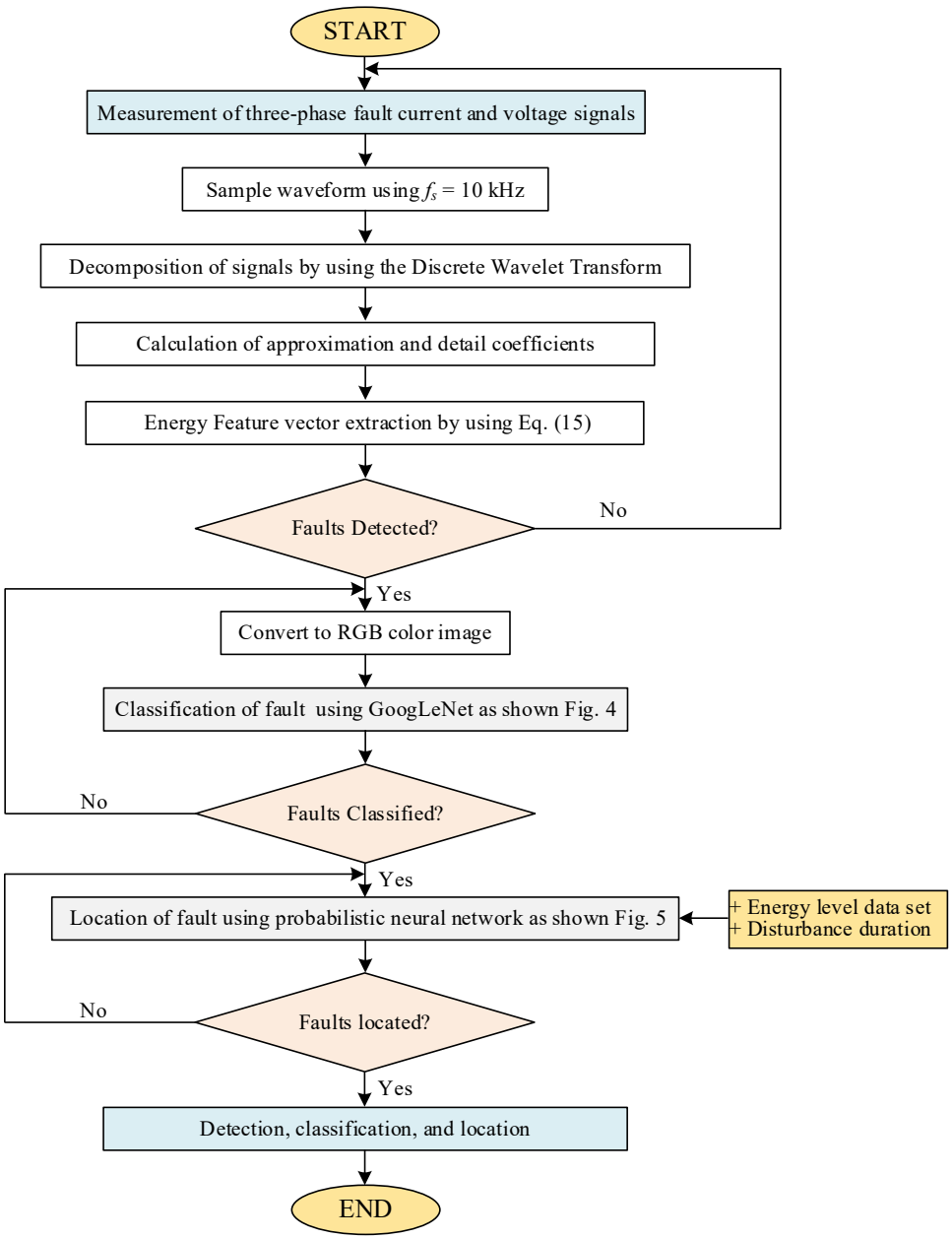

Figure 5. The flowchart of the proposed method to detect, classify, and locate the faults

Step 0: Start

Step 1: Three-phase fault currents and voltage signals at the measurement bus (one of two buses that the transmission line is connected to) are measured via the current transformers (CTs) and voltage transformers (VTs);

Step 2: The high-frequency components for the measured faults current and voltage signals are filtered by the second-order Butterworth to determine the test signals with the sampling frequency of f_s kHz (f_s/50 samples/cycle corresponding to frequency 50 Hz) for the DWT;

Step 3: The DWT-MRA is applied to decompose the one pre- and post-cycle of the fault signals;

Step 4: This step calculates the approximation and detailed coefficients with the aid of Daubechies (db4) mother wavelet through a level decomposition;
Step 5: The detailed energy distribution is calculated by using Eq. (13) to determine the energy feature extraction by Parseval's theorem using Eq. (15);
Step 6: The energy levels, including thirteen energy levels of the current and voltage signals, are compared to detect faults. Detecting the fault types if satisfied, go to Step 7 and vice versa, repeat Step 3;
Step 7: Thirteen energy levels, including current and voltage, are converted to the RGB colour image having size 224×224×3;
Step 8: The fault types are classified by using the GoogLeNet model to train and test the images;
Step 9: If the classification is successful, the next step is to proceed;
Step 10: The fault types are located using PNN, and the energy feature extraction and disturbance duration are calculated by using Eqs. (15) and (12), respectively;
Step 11: If the location is successful, the next step is to proceed
Step 12: The faults are detected, classified, and located.
Step 13: End

4. Results and discussion

A. Power transmission line implementation

In order to evaluate the performance of the proposed method, the 220 kV Hoa Khanh-Hue (HK-H) transmission line with 83.2 km in Figure 6 is considered in this study. This system is a dual circuit connected between HK and H buses. The HK bus is connected to an equivalent 220 kV power grid at the HK substation and a load of 500 MVA, coφ = 0.8. The H bus is connected to an equivalent 220 kV power grid at the H substation and a load of 500 MVA, coφ = 0.8. All relevant parameters are used for simulation shown in Figure 6. The transmission line is modeled as the distributed parameter model. The system and the faults of other types are simulated by using EMTP-RV and MATLAB softwares

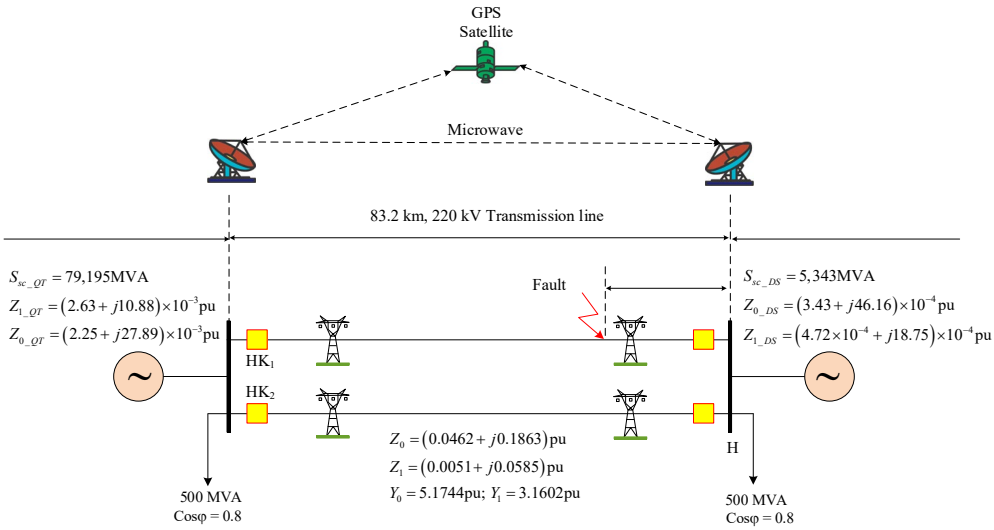

Figure 6. The 220 kV transmission line between Hoa Khanh and Hue substations of Vietnam

B. Fault Detection

For simplicity of simulation and analysis, even cases including the normal case and ten cases of fault are established by a binary code system, as shown in Table 2. The negative sequence voltage and current signals of the fault at both ends of HK and H buses are considered to be synchronized via the global positioning system (GPS).

Table 2. The binary code system of fault types

Outputs	Fault types	Phases			Ground
		A	B	C	G
0	Normal	0	0	0	0
1	AG	1	0	0	1
2	BG	0	1	0	1
3	CG	0	0	1	1
4	AB	1	1	0	0
5	BC	0	1	1	0
6	AC	1	0	1	0
7	ABG	1	1	0	1
8	BCG	0	1	1	1
9	ACG	1	0	1	1
10	ABCG	1	1	1	1

The fault at the F location is created on the transmission line as shown in Figure 6, occurring at 6 ms and is cleared after 1.2 ms. The fault resistance is selected 0 Ohm , and the pre-fault loading condition changes in a range of 5 %. The fault signal with the sampling frequency of 4 kHz corresponding to 80 samples/each cycle is applied to extract and produce training data. The negative sequence voltage signal has been obtained from fault considered as the input of DWT-MRA. The daubechies 4 (db4) mother wavelet is applied to decompose the high-frequency components of this negative sequence voltage signal in one pre- and post-cycles into three detailed coefficients and a third-level approximate coefficient. The analyzed results of the voltage signal, the approximation coefficient of *a3*, the detailed coefficients of *d1-d3*, and the energy distribution of the normal, AG, AB, ABG, and ABCG conditions are shown in Figs. 7-11, respectively.

When applying the proposed DWT-MAR technique, the approximation coefficient of *a3*, the detailed coefficients of *d1-d3*, and the energy distribution clearly detect different fault conditions. These coefficients can clearly discriminate the above-mentioned different fault types that can occur in the transmission line.

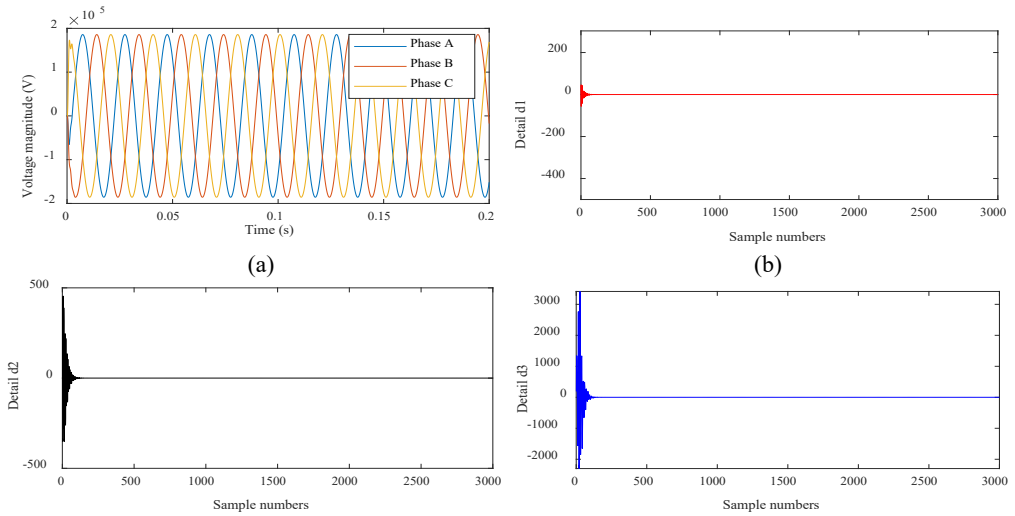

(a) (b) (c) (d)

Figure 7. DWT-MAR in case of the normal: (a) There-phase voltage wave, b) Detailed coefficient 1(*d1*), (c) Detailed coefficient 2 (*d2*), (d) Detailed coefficient 3 (*d3*), (e) Approximation coefficient 3 (*d3*), (f) Energy distribution of phase A current

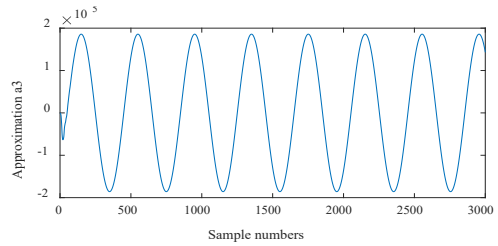

(e)

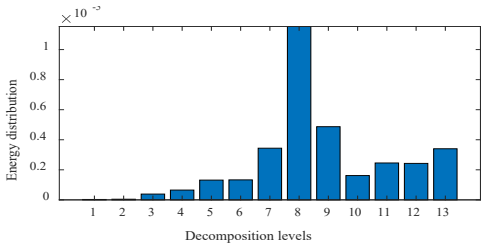

(f)

Figure 7 (cont.)

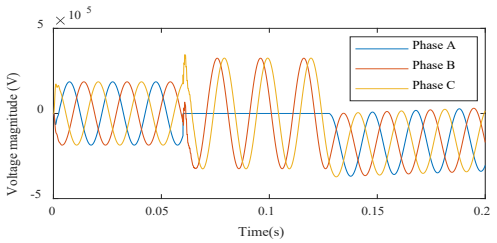

(a)

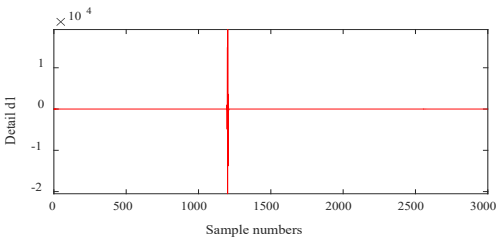

(b)

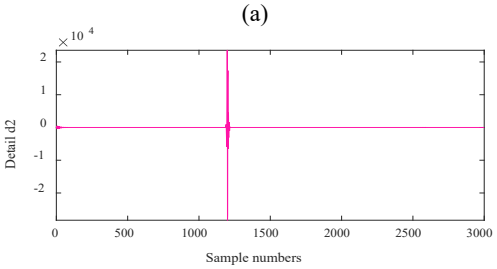

(c)

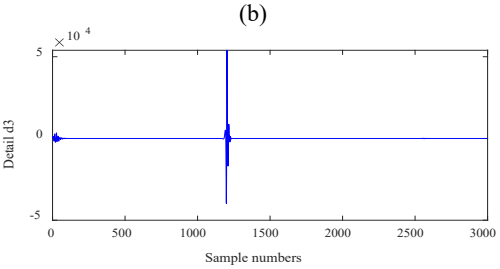

(d)

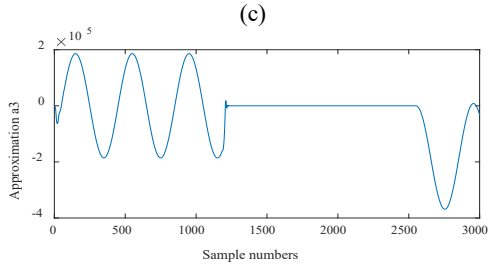

(e)

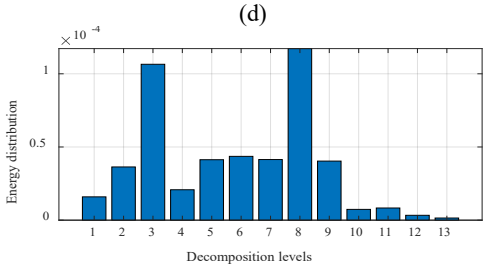

(f)

Figure 8. DWT-MAR in the AG fault: (a) There-phase voltage wave, b) Detailed coefficient 1(*d1*), (c) Detailed coefficient 2 (*d2*), (d) Detailed coefficient 3 (*d3*), (e) Approximation coefficient 3 (*d3*), (f) Energy distribution of phase A current.

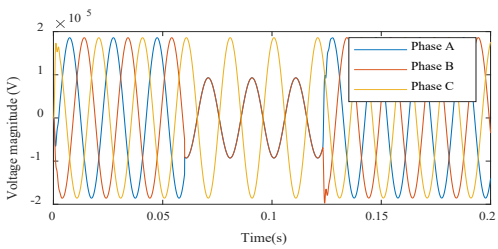

(a)

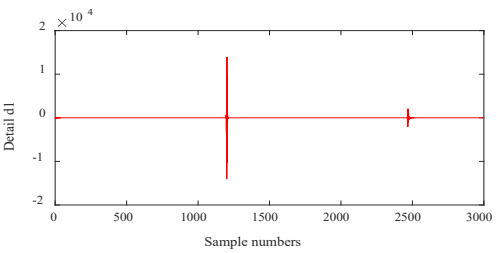

(b)

Figure 9. DWT-MAR in case of the AB fault: (a) There-phase voltage wave, b) Detailed coefficient 1(*d1*), (c) Detailed coefficient 2 (*d2*), (d) Detailed coefficient 3 (*d3*), (e) Approximation coefficient 3 (*d3*), (f) Energy distribution of phase A current

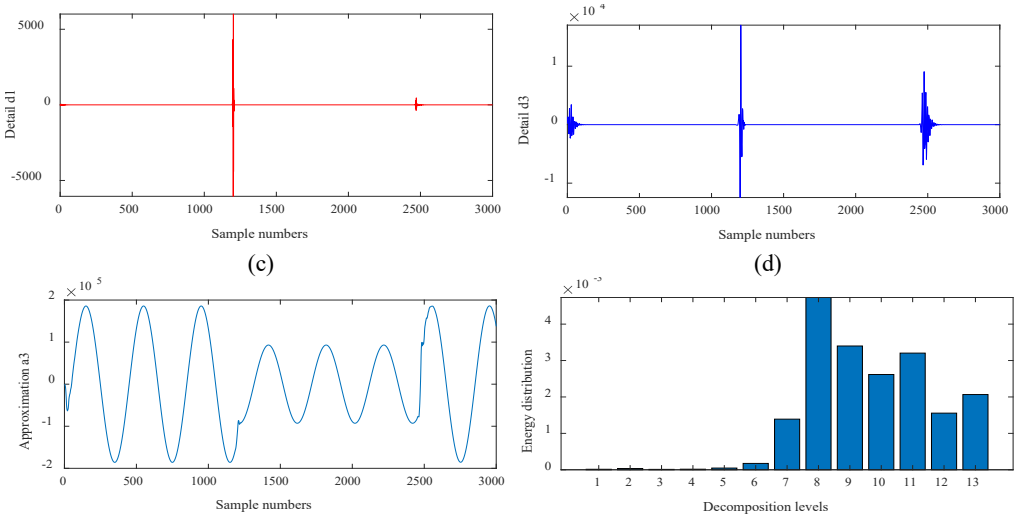

Figure 9. (cont.)

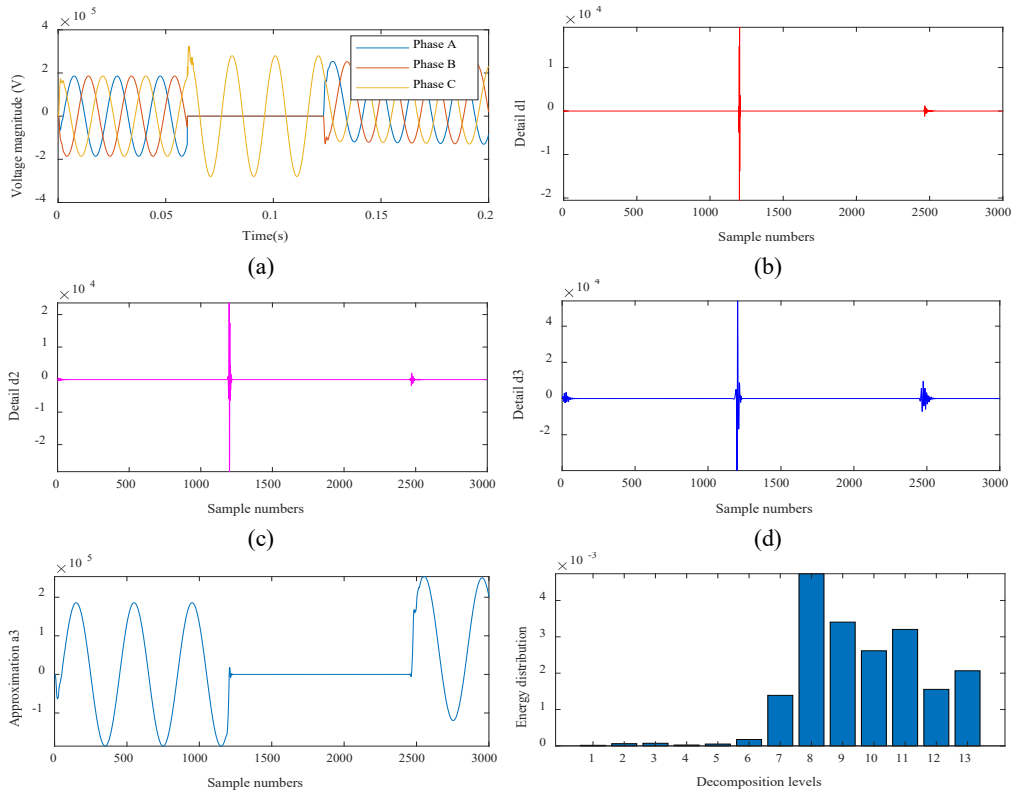

Figure 10. DWT-MAR in case of the ABG fault: (a) There-phase voltage wave, b) Detailed coefficient 1(*d1*), (c) Detailed coefficient 2 (*d2*), (d) Detailed coefficient 3 (*d3*), (e) Approximation coefficient 3 (*d3*), (f) Energy distribution of phase A current

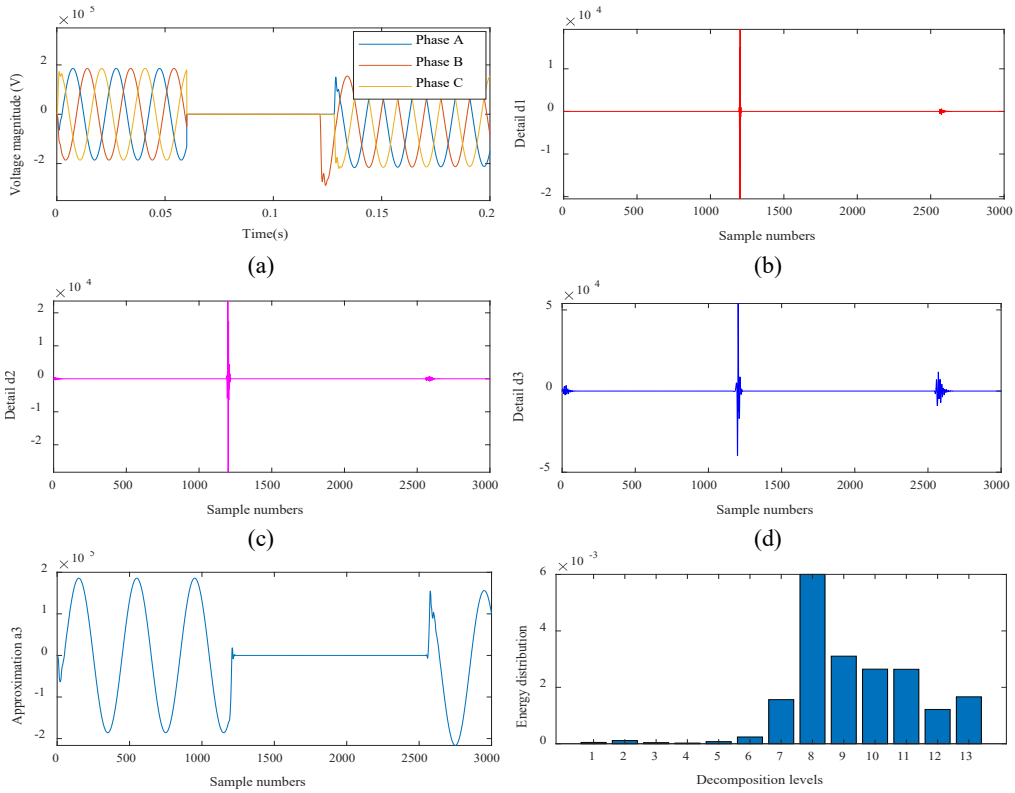

Figure 11. DWT-MAR in the ABCG fault: (a) There-phase voltage wave, b) Detailed coefficient 1(*d1*), (c) Detailed coefficient 2 (*d2*), (d) Detailed coefficient 3 (*d3*), (e) Approximation coefficient 3 (*d3*), (f) Energy distribution of phase A current

C. Fault Classification

Table 3 summarises thirteen energy decomposition levels of each fault type's phase A current signal. Figure 12 (a) shows orderly the energy distributions of four faults under the same three-dimensional. This can clearly observe the differences in energy distribution between different faults. In this paper, after successful fault detection, thirteen energy decomposition levels of each fault type's voltage and current signals are used to convert to the RGB colour images with size 224×224×3. Figure 12 (b) shows the RGB colour images of each fault type that are typical of four out of ten kinds of faults. The RGB colour images are chosen as the input of GoogleNet to perform the classification process.

Table 3. The energy decomposition levels of the phase A current signal of each fault type

Signal types	Energy distribution													Transient period (τ)
	E_1	E_2	E_3	E_4	E_5	E_6	E_7	E_8	E_9	E_{10}	E_{11}	E_{12}	E_{13}	
Nomal	0.14e-7	0.22e-7	3.86e-07	6.53e-07	1.31e-06	1.33e-06	3.43e-06	1.15e-05	4.86e-06	1.62e-06	2.45e-06	2.42e-06	3.40e-06	0.001
SLG	1.59e-5	3.63e-05	1.06e-04	2.07e-05	4.12e-05	4.36e-05	4.14e-05	1.17e-04	4.03e-05	7.37e-06	8.31e-06	3.33e-06	1.47e-06	0.06
LL	2.28e-5	3.43e-05	0.35e-6	0.27e-6	4.73e-05	1.75e-04	1.39E-03	4.73e-03	3.39e-03	2.60e-03	3.20e-03	1.50e-03	2.03e-03	0.06
LLG	3.39e-5	6.09e-05	7.20e-05	2.40e-05	5.08e-05	1.75e-04	1.30E-03	4.70e-03	3.40e-03	2.60e-03	3.20e-03	1.55e-03	2.06e-03	0.06
LLLG	4.7e-5	1.12e-04	3.80e-05	0.52e-7	7.45e-05	1.50e-03	2.39E-04	6.00e-03	3.10e-03	2.60e-03	2.60e-03	1.20e-03	1.60e-03	0.06

Figure13 shows the classification result by testing results through each data of fault type when training the GoogleNet network. The obtained result is the training when using the GoogLeNet network with 210 faulted scenarios corresponding to ten fault types at 21 fault positions on the length of 83.2 km of the proposed transmission line. Figure 13 and Table 4 show that the validation accuracy of training GooleNet is 100%, in which the elapsed time is 4 minutes and 59 seconds, the number of epochs is 20, the number of iterations is 80, the maximum number

of iterations is 80, the iterations per epoch are 4, and the learning rate is constant of 0.0001. The output index of the GoogleNet is 0.9773, 0.7674, 0.7459, 0.6466, and 0.9878, corresponding to the AG, ABG, AB, ABCG fault types and normal case as shown in Figs. 14 (a)-(e), respectively.

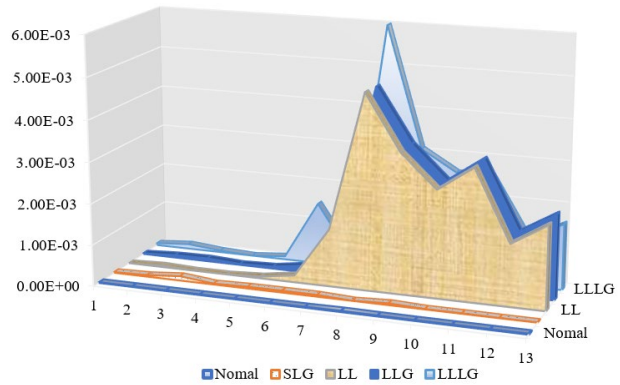

(a)

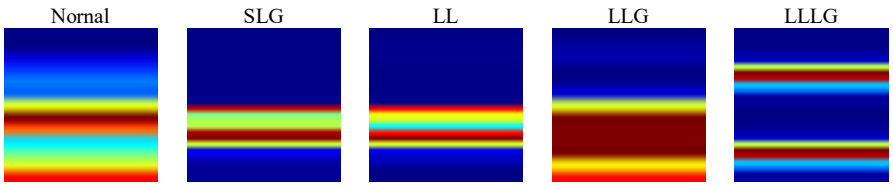

(b)

Figure 12. The energy distributions and its RGB images: (a) the energy distribution of normal and four fault types, (b) corresponding RGB images

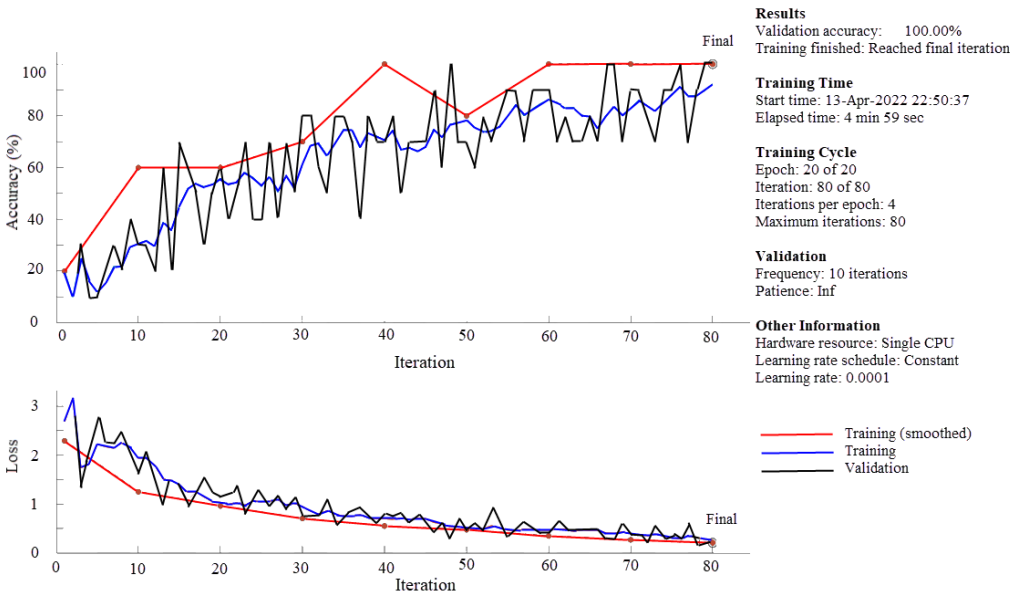

Figure 13. The GoogleNet training result of four out of ten kinds of faults

Table 4. The accurate ratio results of training GoogleNet for four out of ten kinds of faults

Epoch	Iteration	Time elapsed	Mini-batch Accuracy	Validation accuracy	Mini-batch loss	Validation loss	Base Leaning rate
1	1	00:00:09	20.00%	20.00%	2.6780	2.2935	1.0000e-04
3	10	00:00:55	30.00%	60.00%	1.6118	1.2516	1.0000e-04
5	20	00:01:38	60.00%	60.00%	1.1453	0.9610	1.0000e-04
8	30	00:02:14	80.00%	70.00%	0.7685	0.7079	1.0000e-04
10	40	00:02:47	70.00%	100.00%	0.7609	0.5509	1.0000e-04
13	50	00:03:20	70.00%	80.00%	0.4582	0.4736	1.0000e-04
15	60	00:03:53	90.00%	100.00%	0.4031	0.3470	1.0000e-04
18	70	00:04:25	90.00%	100.00%	0.3666	0.2689	1.0000e-04
20	80	00:04:59	100.00%	100.00%	0.2076	0.2076	1.0000e-04

Figure 14. The classification result of four out of ten kinds of faults when using GoogleNet: (a) normal, (b) SLG fault, (c) LLG fault, (d) LL fault, and (e) LLLG fault

D. Fault Location

For the length of 83.2 km of the proposed HK-H transmission line, 21 locations on single-circuit are considered as the fault positions. These locations can happen at the first point 1.6 km from the HK bus to the ending point 1.4 km away from the H bus with a step size of the length of 4 km. Ten different fault types are applied to each location. After successfully detecting and classifying the faults, the PNN method was proposed to process the energy level decomposition of each discrete distorted current and voltage signal of the faults and the transient period of the disturbance. Table 5 presents the results. The result obtained using the proposed method compared to that of the accuracy of the line distance protection REL521 installed at the HK bus.

In order to evaluate the effectiveness of the proposed method for determining the fault location, the condition of the percent distance deviation is considered and can express as follows:

$$\text{Error } \% = \frac{\left|L_{actual} - L_{method}\right|}{L_{total}} \tag{23}$$

where L_{actual} is the actual fault location, L_{method} is either the measured fault location from the relay location REL 521 or the simulated fault location from the proposed method, and L_{total} is the tested total line length.

Table 5 shows that the fault location at # 17 for ABG is the highest error for both the measured fault location from the relay location REL 521 and the simulated fault location from the proposed method. For this fault location, when using the proposed method, the simulated fault location is 64.82 km, and the relay location REL 521 was measured to be 67.2 km, while the actual fault distance is 63.1 km. Therefore, based on the obtained result from Table 5, it can be seen that four locations of fault as # 7, 10, 17, and 21, corresponding to the BCG, BG, ABG, and AG are localized more accurately when using the proposed method compared to the one-terminal one of REL521.

Table 5. The fault location results

Fault location	Fault type	Occurred fault time	Distance of the fault (km)			Error (%)	
			actual fault location	Proposed method	Projected fault location on REL 521	Proposed method	REL521
HK bus	-	-	0.0	-	-	-	-
1	AG	-	1.6	1.53	-	0.08	-
2	BG	-	5.6	5.69	-	0.11	-
3	CG	-	9.6	9.51	-	0.11	-
4	ABG	-	13.6	14.02	-	0.50	-
5	ACG	-	17.6	16.97	-	0.76	-
6	AB	-	21.6	22.01	-	0.49	-
7	BCG	17/5/2011	25.4	26.62	24.1	1.47	1.56
8	AC	-	29.6	28.73	-	1.05	-
9	BC	-	33.6	34.07	-	0.56	-
10	BG	02/8/2010	35.9	36.00	35.8	0.12	0.12
11	ABCG	-	41.6	42.83	-	1.48	-
12	AG	-	45.6	44.75	-	1.02	-
13	CG	-	49.6	48.5	-	1.32	-
14	AB	-	53.6	54.72	-	1.35	-
15	BC	-	57.6	58.82	-	1.47	-
16	AC	-	61.6	62.73	-	1.36	-
17	ABG	12/8/2010	63.1	64.82	67.2	2.07	4.93
18	ACG	-	69.6	70.12	-	0.63	-
19	BCG	-	73.6	72.55	-	1.26	-
20	ABCG	-	74.6	73.12	-	1.78	-
21	AG	20/5/2011	81.8	80.45	83.22	1.62	1.68
H bus	-	-	83.2	-	-	-	-

5. Conclusions

This study has proposed a combination approach using the discrete wavelet transform (DWT), GoogleNet, and probabilistic neural network (PNN) methods for fault diagnosis in the transmission line, in which the DWT one used to detect, the GoogleNet one applied to classify, and the PNN proposed to locate the fault. The measured fault signals of voltage and current of ten fault types in the transmission line from sending or receiving bus are decomposed into the continuous-time in terms of detailed and approximated versions under different frequency resolution levels. For fault identification, the DWT-based multi-resolution analysis (MRA) is used to process the energy distribution during the transient states. After feature extraction, the obtained energy of the subband signal (decomposed by DWT) is transferred under the feature vector form. After successful fault detection, thirteen energy decomposition levels of each fault type's voltage and current signals are converted to the RGB colour images with size 224×224×3. These images are employed as the input of GoogleNet for the fault type classification. After successfully classifying the faults, the PNN method was proposed to process the energy level decomposition of each discrete distorted current and voltage signal of the faults and the transient period of the disturbance. In addition, this paper applied Parseval's theorem to overcome the disadvantages as the memory requirement is large and the recording time is proportional to the size of the sample when using the PNN method.

This study recommends applying the deep learning method to detect, classify, and locate better faults on power transmission lines. It is verifiable through the application on the 220 kV Hoa Khanh-Hue (HK-H) transmission line with 83.2 km of Vietnam under considering the different faults, variable fault resistance between 0 to 5 Ohms, and the changing load of ± 5%. The simulation results show that the proposed method proved effective as it can reduce the error (%) of the fault location compared to the real applied one-terminal method of REL521. Thus, this proposed theory is considered a practical and supportive tool for analyzing the stability of the transmission line system.

Acknowledgment

This work was supported by the Industrial University of Ho Chi Minh City, Ho Chi Minh City, Viet Nam under project no. 21.CNĐ01 (Contract no. 64/HĐ-ĐHCN, March 24, 2022).

Thanks for the support from the Research and Development (R&D) Center of Power Engineering Consulting Joint Stock Company 4 (PECC4) for the research combination as well as everything else.

References

[1]. Ravi. "Causes, Nature and Effect of Fault in Power in Power System 2019" [cited 2019 December 26]; Available from: *http://electricalarticle.com/causes-nature-effect-fault-power-system*.

[2]. L. Eriksson, M. M. Saha and G. D. Rockefeller, "An Accurate Fault Locator with Compensation for Apparent Reactance in the Fault Resistance Resulting from Remote-End Infeed,"*IEEE Power Engineering Review,* vol. PER-5, no. 2, pp. 44-44, Feb. 1985, doi: 10.1109/MPER.1985.5528881.

[3]. T. Kawady and J. Stenzel, "A practical fault location approach for double circuit transmission lines using single end data," *IEEE Transactions on Power Delivery,* vol. 18, no. 4, pp. 1166-1173, Oct. 2003, doi: 10.1109/TPWRD.2003.817503.

[4]. V. P. Huan, L. K. Hung, and N. H. Viet, "Fault Classification and Location on 220kV Transmission line Hoa Khanh – Hue Using Anfis Net," *Jounal of Automation and Control Engineering,* vol. 3, no. 2, pp. 98-104, April, 2015. doi: 10.12720/joace.3.2.98-104.

[5]. A. Yadav and A.S. Thoke, "Transmission line fault distance and direction estimation using artificial neural network," *International Journal of Engineering, Science and Technology,* vol. 3, no. 8, pp.110-21, 2011, doi: 10.4314/ijest.v3i8.9.

[6]. C. S. Yu, C. W. Liu, S. L. Yu and J. A. Jiang, "A new PMU-based fault location algorithm for series compensated lines," *IEEE Transactions on Power Delivery,* vol. 17, no. 1, pp. 33-46, Jan. 2002, doi: 10.1109/61.974185.

[7]. E.E. Ngu and K. Ramar, "A combined impedance and traveling wave based fault location method for multi-terminal transmission lines," *International Journal of Electrical Power & Energy Systems,* vol. 33, no. 10, pp.1767-1775, Dec. 2011, doi: 10.1016/j.ijepes.2011.08.020.

[8]. K. Saravanababu, P. Balakrishnan and K. Sathiyasekar, "Transmission line faults detection, classification, and location using Discrete Wavelet Transform," *2013 International Conference on Power, Energy and Control (ICPEC),* pp. 233-238, 2013, doi: 10.1109/ICPEC.2013.6527657.

[9]. O. A. S. Youssef, "Online applications of wavelet transforms to power system relaying," in *IEEE Transactions on Power Delivery,* vol. 18, no. 4, pp. 1158-1165, Oct. 2003, doi: 10.1109/TPWRD.2003.817487.

[10]. O.O. Kalu and T.C. Madueme, "Application of artificial neural network (ANN) to enhance power systems protection: a case of the Nigerian 330 kV transmission line," *Electrical Engineering,* vol. 100, no. 3, pp. 1467-79, Sep. 2018, doi: 10.1007/s00202-017-0599-y.

[11]. M. Jamil, R. Singh, and S. K. Sharma, "Fault identification in electrical power distribution system using combined discrete wavelet transform and fuzzy logic," *Journal of Electrical Systems and Information Technology,* vol 2, no. 2, pp. 257-67, Sep. 2015, doi: 10.1016/j.jesit.2015.03.015.

[12]. P. Ray, D. P. Mishra and S. Mohaptra, "Fault classification of a transmission line using wavelet transform & fuzzy logic," *2016 IEEE 1st International Conference on Power Electronics, Intelligent Control and Energy Systems (ICPEICES),* pp. 1-6, July 2016, doi: 10.1109/ICPEICES.2016.7853293.

[13]. K.Hosseini, "Short circuit fault classification and location in transmission lines using a combination of wavelet transform and support vector machines," *International Journal on Electrical Engineering and Informatics,* vol. 7, no. 2, p. 353, 2015, doi: 10.15676/ijeei.2015.7.2.14.

[14]. M. Coban and S. S. Tezcan, 'Detection and classification of short-circuit faults on a transmission line using current signal,' *Bulletin of the Polish Academy of Sciences Technical Sciences*, vol. 69, no. 4, 2021, pp. 1-9, doi: 10.24425/bpasts.2021.137630.

[15]. I. Baqui, I. Zamora, J. Mazón, and G. Buigues, "High impedance fault detection methodology using wavelet transform and artificial neural networks," *Electric Power Systems Research,* vol. 81, no. 7, pp.1325-33, Jul 2011, doi: 10.1016/j.epsr.2011.01.022.

[16]. H. Khorashadi-Zadeh and M. R. Aghaebrahimi, "A novel approach to fault classification and fault location for medium voltage cables based on artificial neural network," *International journal of computational intelligence*, vol. 2, no. 2, pp. 90-93, Jan. 2006.

[17]. A. Raza, A. Benrabah, T. Alquthami, and M. A. Akmal , "Review of fault diagnosing methods in power transmission systems,' Applied Sciences. vol. 10, no. 4, p. 1312, Jan. 2020, doi: 10.3390/app10041312.

[18]. A. Mukherjee, P.K. Kundu, A. Das, "Transmission line faults in power system and the different algorithms for identification, classification and localization: a brief review of methods," *Journal of The Institution of Engineers (India): Series B*, vol. 102, no. 4, pp. 855-77, Aug. 2021, doi: 10.1007/s40031-020-00530-0.

[19]. M. H. Wang, S. D. Lu and R. M. Liao, "Fault Diagnosis for Power Cables Based on Convolutional Neural Network With Chaotic System and Discrete Wavelet Transform," *IEEE Transactions on Power Delivery*, vol. 37, no. 1, pp. 582-590, Feb. 2022, doi: 10.1109/TPWRD.2021.3065342.

[20]. V. Vanitha and M. G. Hussien, "Framework for Transmission Line Fault Detection in a Five Bus System Using Discrete Wavelet Transform," *Distributed Generation & Alternative Energy Journal*, vol. 37, no. 3, pp. 525-536, 2022 doi: 10.13052/10.13052/dgaej2156-3306.3737.

[21]. X. Glorot, A. Bordes, Y. Bengio, "Deep sparse rectifier neural networks," Proceedings of the fourteenth international conference on artificial intelligence and statistics, pp. 315-323, Jun. 2011.
[22]. S.Arora, A. Bhaskara, R. Ge, and T. Ma, "Provable bounds for learning some deep representations," *In International conference on machine learning*, pp. 584-592, Jan. 2014.
[23]. S. Han, H. Mao, and W. J. "Dally Deep compression: Compressing deep neural networks with pruning, trained quantization and huffman coding," *arXiv preprint arXiv:1510.00149.* Oct. 2015, doi:10.48550/arXiv.1510.00149.
[24]. G. Cao, K. Zhang, K. Zhou, H. Pan, Y. Xu and J. Liu, "A Feature Transferring Fault Diagnosis based on WPDR, FSWT and GoogLeNet," *2020 IEEE International Instrumentation and Measurement Technology Conference*, pp. 1-6, 2020, doi: 10.1109/I2MTC43012.2020.9129483.
[25]. E. R. Yilmaz and M. A.Trocan, "A modified version of GoogLeNet for melanoma diagnosis," *Journal of Information and Telecommunication, vol. 5, vol. 3, pp. 395-405, Jul. 2021, doi:* 10.1080/24751839.2021.1893495.
[26]. D. F. Specht, "Probabilistic neural networks," Neural networks, vol. 3, no. 1, pp.109-118, Jan. 1990, doi: 10.1016/0893-6080(90)90049-Q.
[27]. M. N. Akram and S. Lotfifard, "Modeling and Health Monitoring of DC Side of Photovoltaic Array," *IEEE Transactions on Sustainable Energy*, vol. 6, no. 4, pp. 1245-1253, Oct. 2015, doi: 10.1109/TSTE.2015.2425791.
[28]. N. Huang, D. Xu, X. Liu, and L. Lin, "Power quality disturbances classification based on S-transform and probabilistic neural network," *Neurocomputing*, vol. 98, pp.12-23, Dec. 2012, doi: 10.1016/j.neucom.2011.06.041.
[29]. M. Manjula, S. Mishra, A. V. Sarma, "Empirical mode decomposition with Hilbert transform for classification of voltage sag causes using probabilistic neural network," *International Journal of Electrical Power & Energy Systems*, vol. 44, no. 1, pp. 597-603, jan 2013, doi: 10.1016/j.ijepes.2012.07.040.
[30]. S. Wang and H. Chen, "A novel deep learning method for the classification of power quality disturbances using deep convolutional neural network," *Applied energy*, vol. 235, pp. 126-40, Feb. 2019, doi: 10.1016/j.apenergy.2018.09.160.
[31]. Y. Shen, M. Abubakar, H. Liu, and F. Hussain, "Power quality disturbance monitoring and classification based on improved PCA and convolution neural network for wind-grid distribution systems," *Energies*, vol. 12, no. 7, p. 1280, Jan, 2019, doi: 10.3390/en12071280.
[32]. T. M. Lai, L. A. Snider, E. Lo and D. Sutanto, "High-impedance fault detection using discrete wavelet transform and frequency range and RMS conversion," *IEEE Transactions on Power Delivery*, vol. 20, no. 1, pp. 397-407, Jan. 2005, doi: 10.1109/TPWRD.2004.837836.
[33]. C. Szegedy, W. Liu, Y. Jia, P. Sermanet, S. Reed, D. Anguelov, D. Erhan, V. Vanhoucke and A. Rabinovich, "Going deeper with convolutions," *Proceedings of the IEEE conference on computer vision and pattern recognition,* pp. 1-9, 2015, doi: 10.1109/CVPR.2015.7298594.
[34]. Z. L. Gaing, "Wavelet-based neural network for power disturbance recognition and classification," *IEEE Transactions on Power Delivery,* vol. 19, no. 4, pp. 1560-1568, Oct. 2004, doi: 10.1109/TPWRD.2004.835281.

Le Van Dai received MSc degree in Electrical Engineering from the Ho Chi Minh City University of Technology, Vietnam, in 2008. He received his Ph.D. degree in Information and electricity engineering from Hunan University, Changsha, China, in 2016. Since 2011, he has been a lecturer at the Faculty of Electrical Engineering Technology and Header of the Electric Power System Research Group, Industrial University of Ho Chi Minh City, Vietnam. His research interests include system power research as stability, protection, power quality, and the grid-connected control of solar photovoltaics and wind power energy conversion systems.

Le Cao Quyen received the B.Sc. and M.Sc. degrees from the Ho Chi Minh City University of Technology, Vietnam, in 1999 and 2005, respectively. He received his Ph.D. degree in Electrical Engineering from Danang University, Vietnam, in 2012. Since 2022 he has been working as Chairman of the Board of the Power Engineering Consulting Joint stock Company 4, Vietnam (EVNPECC4). His research interests include the grid-connected control of renewable energy and power system stability analysis and calculation.

Nhan Bon Nguyen received B.Sc. and M.Sc. degrees from the Ho Chi Minh City University of Technology, Vietnam (the member of Vietnam National University – Ho Chi Minh city) in 1996 and 2000, respectively. He received his Ph.D. degree in Electrical Engineering from the Ho Chi Minh City University of Technology in 2015. He is currently working as a senior lecturer in the Department of Electrical and Electronics Engineering of Ho Chi Minh City University of Technology and Education. His research interests include intelligent methods for power system protection, power quality, power system transients, and Smart Grids-related studies.